DALTON
FULL PAPER

Spectroelectrochemical and computational studies of tetrachloro and tetrabromo oxo- and nitrido-technetium(V) and their Tc^{VI} counterparts‡

John Baldas,[a] Graham A. Heath,*[,b] Stuart A. Macgregor,†[,b] Klaus H. Moock,[b] Sandra C. Nissen[b] and Raphael G. Raptis[c]

[a] *Australian Radiation Laboratory, Yallambie, Victoria 3085, Australia*
[b] *Research School of Chemistry, Australian National University, Canberra ACT 0200, Australia*
[c] *Chemistry Department, University of Puerto Rico, San Juan, P.R. 00931-3346*

The technetium complexes $[NBu_4][Tc^{VI}NX_4]$ and $[NBu_4][Tc^{V}OX_4]$ (X = Cl or Br) have been studied by electrochemical and theoretical methods. The redox potentials of the halide complexes are strongly affected by the introduction of axial O^{2-} or N^{3-} ligands. The $Tc^{VI/V}$ couple decreases from +1.84 V for $[TcOCl_4]^{0/-}$ to +0.21 V for $[TcNCl_4]^{-/2-}$. *In situ* spectroelectrochemical techniques were employed to characterise d^1 $Tc^{VI}OCl_4$ (by oxidation) and d^2 $[Tc^{V}NX_4]^{2-}$ (by reduction) in solution. However, the oxidation of $[TcOBr_4]^-$ at +1.73 V is chemically irreversible. The featureless visible spectra of the Tc^{V} species contrast markedly with the wealth of charge-transfer bands found for the Tc^{VI} chromophores. In-plane $\{X_4\} \longrightarrow Tc^{VI}$ (d_{xy}) transitions are precluded by the low-spin $(d_{xy})^2$ configuration induced by the axial perturbation (by O^{2-} or N^{3-}) of the d_π levels. Density functional calculations were used to analyse the trend in redox potentials and electronic spectra, and, in particular, to resolve additional complexities of the visible CT spectra of the five-co-ordinate d^1 $[TcNX_4]^-$ (X = Cl or Br) dissolved in non-co-ordinating solvents. These relatively complicated spectra closely resemble the visible reflectance spectra measured for the unambiguously five-co-ordinate $[NBu_4][TcNX_4]$ salts in the solid state, whereas the absorption spectra of the nitrido complexes dissolved in aqueous HX suggest the presence of the corresponding six-co-ordinate d^1 *trans*-$[TcNX_4(H_2O)]^-$ complex.

Among technetium halide complexes, the tetrachloro and tetrabromo nitrido Tc^{VI} compounds have received particular attention because of their structural and spectroscopic properties, and their isoelectronic relationship with topical oxo–Mo^{V} centres.[1]

Recently, we examined the impact of the differing donor properties of the O^{2-} and N^{3-} ligands on the isovalent octahedral or pseudo-octahedral complexes MCl_6, $[MOCl_5]^-$ and $[MNCl_4]^-$ (M = Mo or W).[2] In the present work, these investigations have been extended to the related technetium nitrido[3] and oxo[4] complexes, $[TcNX_4]^-$ and $[TcOX_4]^-$ (X = Cl or Br). We have measured the electrode potentials of these compounds in strictly anhydrous media, and determined their UV/VIS spectra in successive oxidation states, using spectroelectrochemical techniques. This is a valuable strategy because of the underlying relationship between metal-centred electrode potentials and optical charge-transfer (XMCT) spectra in systems where the pertinent optical acceptor orbital is also reliably identified as the redox-active orbital.[5] Earlier investigations illustrated the correlation between XMCT spectra and $Ru^{III/II}$ electrode potentials for the related sequence of d^5 chromophores $[RuX_6]^{3-}$, $[RuX_5L]^{2-}$, *trans*-$[RuX_4L_2]^-$ (where L = RCN).[5,6] The contrasting electronic spectra of $[TcNX_4]^-$ (X = Cl or Br), when dissolved in concentrated HX or MeCN, have been reported previously but the origin of this difference remained unsettled.[1]

Previous EPR studies of d^1 $[MoOX_4]^-$ and $[TcNX_4]^-$ complexes have established that the unpaired electron resides in the $2b_2$ (d_{xy}) orbital.[3,7] Oxo and nitrido complexes of the form MYX_n (M = Mo, W, Re or Os; X = F or Cl; n = 3–5) have been studied by quantum mechanical *ab initio* methods at the H–F and MP2 level, with a view to interpreting the nature of the M–Y bond and matching its vibrational frequency.[8] Single crystals of $[AsPh_4][TcNCl_4]^-$, prepared by Baldas *et al.*,[3] have been studied by polarised neutron diffraction experiments to determine the spin-density distribution, and the results compared with theoretical calculations and EPR data.[9]

As in the Mo and W study,[2] and in subsequent theoretical analysis[10] of a wider range of $[MX_6]^{z-}$ (X = F or Cl) complexes showing periodic progressions[11,12] in their d^n/d^{n+1} couples, density functional calculations have been employed to reinforce our understanding of the experimental redox data. The calculations were also crucial in assigning the intense charge-transfer features of the UV/VIS spectra which change markedly between Tc^{V} and Tc^{VI}, and between the oxo- and nitrido-chromophores. In addition we have examined the unusual qualitative variation in the CT manifold of d^1 $[TcNX_4]^-$ in different environments, prompted by the discovery that solutions of the nitrido complexes in strictly anhydrous and poorly co-ordinating CH_2Cl_2 electrolyte mixtures have UV/VIS spectra that are virtually indistinguishable from those observed in MeCN.

Results

Voltammetry and spectroelectrochemistry

In the stringently dried inert solvent–electrolyte system (NBu_4PF_6–CH_2Cl_2) employed in this work, all the compounds studied were found to be stable at room temperature in their most accessible oxidation state. Electrochemical experiments were carried out in a specially designed evacuable electrochemical cell described previously,[13] while electronic spectra were recorded using a cryostatted optically transparent thin-layer electrode (OTTLE) cell. The voltammetric data are summarised in Table 1 together with the relevant data for related

† *Present address*: Department of Chemistry, Heriot-Watt University, Edinburgh, UK EH14 4AS.
‡ *Non-SI unit employed*: eV ≈ 1.602×10^{-19} J.

Table 1 Voltammetric data for the compounds[a]

Compound	$E_{\frac{1}{2}}$/V[b] $M^{7+/6+}$	$M^{6+/5+}$	$M^{5+/4+}$
$[NBu_4][TcOCl_4]$		+1.84	−0.52[c]
$[NBu_4][TcOBr_4]$		+1.73[d]	−0.39[e]
$[NBu_4]_2[MoOCl_5]$[f]		+1.70	−0.65
$[NBu_4][TcNCl_4]$	+2.7[g]	+0.21	
$[NBu_4][TcNBr_4]$		+0.32	
$[NBu_4][MoNCl_4]$[f]		+0.25	−1.80

[a] At a platinum electrode in CH_2Cl_2 containing 0.5 M NBu_4PF_6 electrolyte, referred to SCE such that $E_{\frac{1}{2}} = +0.48$ V for $[Fe(C_5H_5)_2]^{+/0}$. [b] Reversible conditions at a scan rate $v = 100$ mV s^{-1} at 298 K unless otherwise noted. [c] Cathodic peak potential, E_a; irreversible behaviour for CV and a.c. experiment. [d] Small return wave in CV at 500 mV s^{-1} and 230 K; a.c. signal at +1.73 V. [e] Irreversible behaviour for CV; small a.c. signal at −0.39 V. [f] From ref. 2. [g] Anodic peak potential E_c; irreversible behaviour for CV and a.c. (+2.65 V) experiment.

molybdenum complexes. Table 2 lists the electronic absorption data for all four compounds in oxidation states V and VI (apart from inaccessible $TcOBr_4$).

For the five-co-ordinate Tc species under discussion, deliberate addition of dry solid NBu_4X to the test solutions did not alter the optical spectra or the electrode potentials, or produce any additional voltammetric signals (except waves typical of free halide oxidation). Thus, six-co-ordinate species of the form $[TcYX_5]^{2-}$ are apparently not formed in discernible amounts during the electrochemical experiments (even for Tc^{VI}) and no evidence was seen for equilibrium (1) considered elsewhere.[14,15]

$$[TcYX_4]^- + X^- \rightleftharpoons [TcYX_5]^{2-} \quad (Y = N \text{ or } O;\ X = Cl \text{ or } Br) \quad (1)$$

Strong support for retention of strict five-co-ordinate geometry by $[TcNX_4]^-$ in CH_2Cl_2 electrolyte solutions (and even in MeCN) was obtained from comparisons with the visible reflectance spectra of powdered samples of $[NBu_4][TcNX_4]$ (X = Cl or Br), which were prepared by literature methods.[4,16]

$[NBu_4][TcNCl_4]$ and $[NBu_4][TcNBr_4]$. Solutions of the nitrido complexes $[TcNCl_4]^-$ and $[TcNBr_4]^-$ in the electrochemical media are orange-red and intensely blue, respectively. Their redox behaviour can be formulated in terms of a Tc^{VI} metal centre ($4d^1$), formally bearing an N^{3-} ligand. Fig. 1 shows the cyclic and a.c. voltammograms of $[NBu_4][TcNCl_4]$ in CH_2Cl_2. A fully reversible one-electron reduction, $[TcNX_4]^{-/2-}$ ($4d^1/4d^2$), is observed at $E_{\frac{1}{2}} = +0.21$ V (*vs.* SCE) for the chloro and at $E_{\frac{1}{2}} = +0.32$ V for the bromo complex (Table 1). No further reduction steps were observed for either system to the limit of solvent electrolysis (−2.8 V). An irreversible oxidation corresponding to $[TcNCl_4]^{0/-}$ ($4d^0/4d^1$) is found at +2.7 V (anodic peak potential). The analogous oxidation step for the bromo species is obscured by complicated anodic processes, probably associated with the ligand-based oxidation of Br^- from the $\{NBr_4\}$ ligand set. Thus, the accessible electrode processes can be summarized as in equation (2).

$$\underset{d^0(Cl\ only)}{TcNX_4} \xleftarrow{-e} \underset{d^1}{[TcNX_4]^-} \underset{-e}{\overset{+e}{\rightleftharpoons}} \underset{d^2}{[TcNX_4]^{2-}} \text{—//→} \quad (2)$$

The reversibility of the $[TcNX_4]^{-/2-}$ reductions allowed the *in situ* electrochemical generation and characterisation of $[TcNX_4]^{2-}$ species in an N_2-purged thin-layer cell. Fig. 2(a) and 2(b) compare the spectral changes that occur upon reduction of $[NBu_4][TcNCl_4]$ and $[NBu_4][TcNBr_4]$ at 218 K. Even under these conditions, $[TcNBr_4]^{2-}$ showed signs of slow decomposition, whereas $[TcNCl_4]^{2-}$ appeared stable over a period of 24 h.

The spectrum of orange d^1 $[TcNCl_4]^-$ in CH_2Cl_2 contains

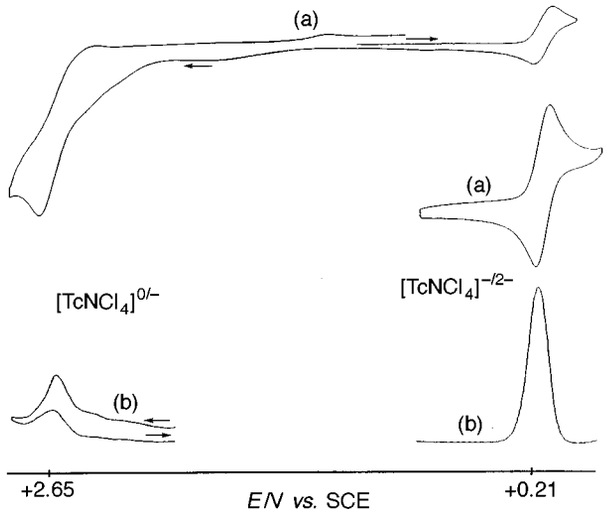

Fig. 1 Cyclic (a) and alternating current (b) voltammograms of $[NBu_4][TcNCl_4]$ in CH_2Cl_2–NBu_4PF_6 solution

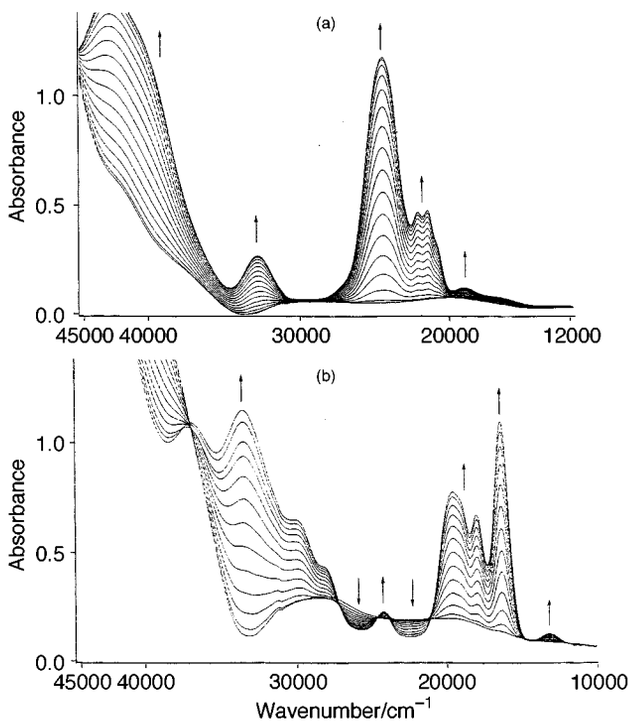

Fig. 2 Spectroelectrochemical monitoring of the reversible reduction of (a) $[TcNCl_4]^-$ to $[TcNCl_4]^{2-}$ and (b) $[TcNBr_4]^-$ to $[TcNBr_4]^{2-}$ in CH_2Cl_2–NBu_4PF_6 solution at 218 K. N.B. Regeneration of Tc^{VI} shown in both cases

four relatively intense bands. The lowest of these, centred at 21 800 cm^{-1}, exhibits distinctive fine structure. A further weak band is observed at 19 100 cm^{-1}. Upon reduction to Tc^V (d^2), all these bands collapse and the final spectrum is essentially featureless below 35 000 cm^{-1}. As a consequence, $[TcNCl_4]^{2-}$ is almost colourless. This is unusual for chloro- and bromo-complexes of a high-valent transition metal with an incomplete $d\pi$ subshell, such as Tc^V (d^2), which might ordinarily be expected to yield a wealth of low-energy XMCT bands. Comparable behaviour for the corresponding Tc^V oxo compounds is described below.

The spectrum of $[TcNBr_4]^-$ is closely related to that of $[TcNCl_4]^-$ but consistently red-shifted by about 5000 cm^{-1}, especially when the centre of gravity of each band manifold is considered (see later Discussion). Electrogenerated $[TcNBr_4]^{2-}$, like $[TcNCl_4]^{2-}$, is almost colourless [*cf.* Fig. 2(b)], with no prominent bands until well above 30 000 cm^{-1}. The broad

Table 2 Spectral data for $[TcOX_4]^z$ and $[TcNX_4]^z$ (X = Cl or Br; $z = 0$, 1− or 2−)

Compound	ν/cm^{-1} (ε/M^{-1} cm^{-1})									
$[TcOCl_4]^-$ [a]	42 200 (sh)	33 330 (5 900)	27 660 (1 200)	21 400 (14)	17 000 (3)	11 200 (11)				
$[TcOCl_4]$ [b]	40 980 (16 000)	31 000 (sh)	28 120 (7 200)	25 000 (sh)	17 230 (4 000)	11 300 (80)				
$[TcOBr_4]^-$ [a]	39 800 (8 200)	33 700 (sh)	28 100 (4 000)	22 100 (110)	16 200 (11)					
$[TcNCl_4]^-$ [a]	43 110 (9 000)	33 340 (1 700)	24 580 (6 400)	22 220 (2 300)	21 570 (2 300)	20 900 (sh)	19 100 (280)	11 900 (40)		
$[TcNCl_4]^-$ [c]		33 015 (1.5)	24 505 (3.1)	22 015 (2.4)	21 465 (2.6_5)	20 700 (sh)	18 935 (0.6)			
$[TcNCl_4]^{2-}$ [b]	43 500 (sh)	19 890 (260)								
$[TcNBr_4]^-$ [a]	37 120 (5 100)	33 940 (5 900)	30 500 (sh)	28 600 (sh)	24 380 (600)	19 570 (3 200)	19 200 (sh)	17 980 (2 700)	16 320 (4 800)	13 180 (100)
$[TcNBr_4]^-$ [c]		33 215 (1.1)	30 000 (sh)	28 000 (sh)	24 440 (0.4_5)	19 920 (1.1)	19 265 (1.1)	17 890 (1.1_5)	16 185 (1.3_5)	13 105 (0.2)
$[TcNBr_4]^{2-}$ [b]	40 650 (10 000)	28 700 (1 000)	19 000 (sh)							

[a] At 218 K in CH_2Cl_2 containing 0.5 M NBu_4PF_6. [b] Spectrum obtained by *in situ* electrogeneration under the same conditions. [c] Solid-state diffuse reflectance spectra, numbers in parentheses are relative peak heights.

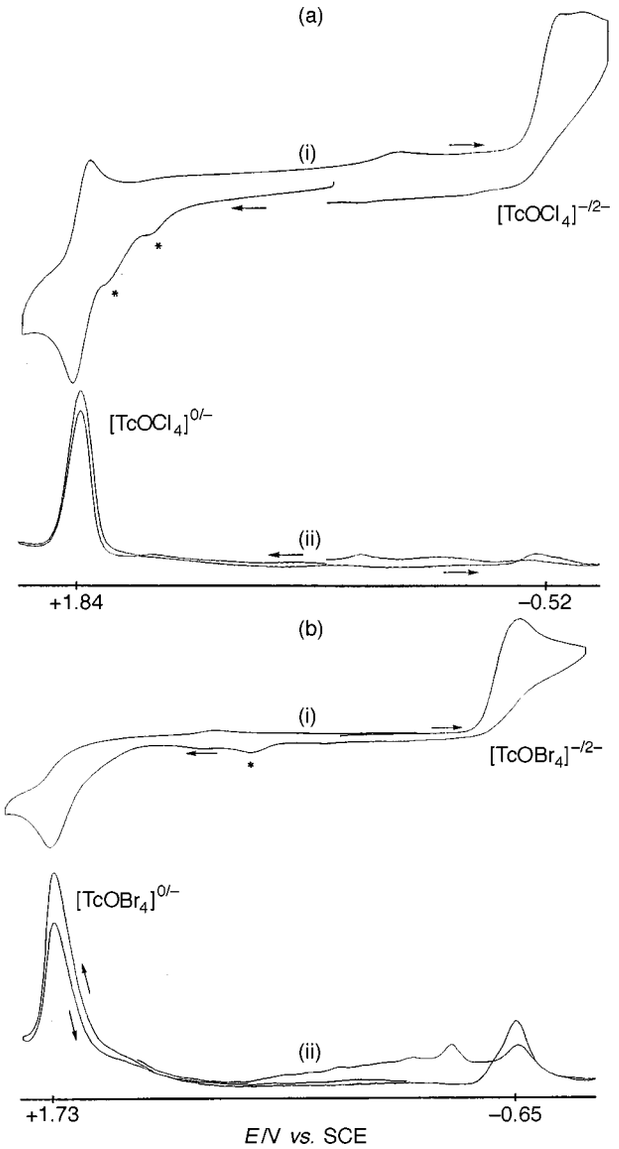

Fig. 3 (a) Cyclic (i) and alternating current (ii) voltammogram of $[NBu_4][TcOCl_4]$ in CH_2Cl_2–NBu_4PF_6 solution. Oxidation process of free Cl^- (*) observable in the CV. (b) Cyclic (i) and alternating current (ii) voltammogram of $[NBu_4][TcOBr_4]$ in CH_2Cl_2–NBu_4PF_6 solution. Oxidation process of free Br^- (*) observable in the CV

absorptions near 20 000 and 30 000 cm^{-1} are connected with the slow decomposition of $[TcNBr_4]^{2-}$, mentioned above. Less clear-cut deviations in the base-line are also seen for $[TcNCl_4]^{2-}$, in Fig. 2(a). Further experiments are required to clarify the possibility of weak (d–d) Tc^V bands falling in this region; fortunately the spectral definition of the Tc^{VI} species seems unimpaired.

Reflectance spectra for powdered $[NBu_4][TcNCl_4]$ and $[NBu_4][TcNBr_4]$ in the region 5000 to 35 000 cm^{-1} were recorded and are detailed in Table 2. The spectra are well resolved and, as can be seen from the comparison in Table 2, correspond closely to those recorded for the electrolyte solutions.

$[NBu_4][TcOCl_4]$ and $[NBu_4][TcOBr_4]$. Fig. 3(a) and 3(b) compare the cyclic and a.c. voltammograms of $[NBu_4][TcOCl_4]$ and $[NBu_4][TcOBr_4]$. A reversible one-electron oxidation process is observed for $[NBu_4][TcOCl_4]$ at $E_{\frac{1}{2}} = +1.84$ V, corresponding to the Tc^{VI}/Tc^V ($4d^1/4d^2$) redox couple. This is consistent with an earlier report of the existence of light-sensitive $TcOCl_4$.[17] The corresponding one-electron oxidation of $[TcOBr_4]^-$ is defined best by its quasi-reversible a.c. peak, located at +1.73 V. The process appears irreversible by cyclic

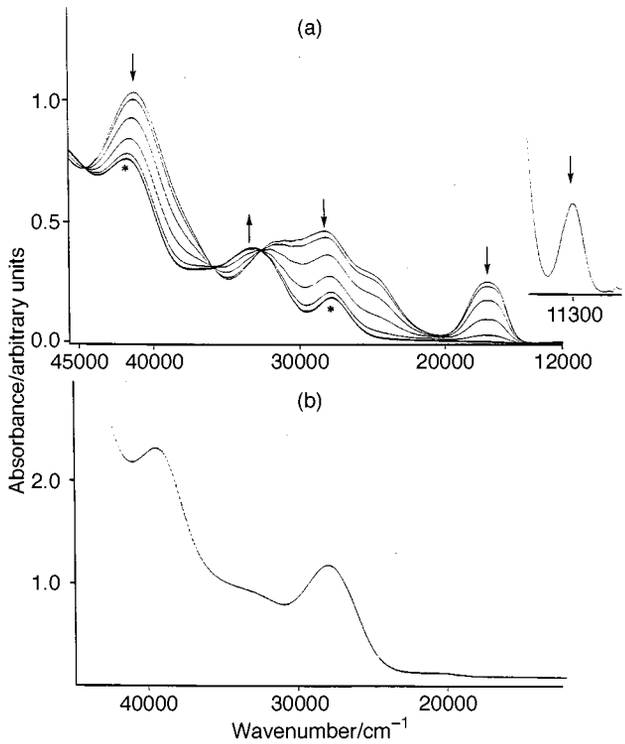

Fig. 4 (a) Spectroelectrochemical monitoring of the reversible oxidation of $[TcOCl_4]^-$ to $TcOCl_4$ in CH_2Cl_2–NBu_4PF_6 solution at 218 K. N.B. Regeneration of Tc^V is shown (* indicates position of possible $[TcCl_6]^{2-}$ contributions); (b) UV/VIS spectrum of $[TcOBr_4]^-$ at 298 K

voltammetry (in lacking a return wave) at scan rates slower than 100 mV s^{-1}. However, at scan rates faster than 500 mV s^{-1} at 213 K, a small return component is observed, and the overall CV wave is consistent with the position of the a.c. signal. Thus in the $[TcYX_4]^{z-}$ systems, the d^1/d^2 couple is displaced by *ca.* 1.5 V between analogous nitrido and oxo complexes (*cf.* Fig. 1 and Fig. 3).

According to cyclic voltammetry, the $[TcOX_4]^{-/2-}$ reduction process (d^2/d^3) appears to be chemically irreversible for both halides, with the cathodic peak potentials located at −0.52 (Cl) and −0.39 V (Br) respectively. The $[TcOBr_4]^{-/2-}$ reduction shows a distinct a.c. voltammetric response, not observed for the chloro analogue. For both complexes the reductive process is apparently accompanied by dissociation of X^-, indicated by the emergence of characteristic signals on the return scan corresponding to oxidation of free Cl^- or Br^-. Despite this, the voltammetric reversibility of the $[TcOX_4]^{-/2-}$ couple was not improved by the addition of halide in the form of anhydrous NBu_4X to the electrolyte medium [see equation (3)].

$$\leftarrow\!/\!/\!\!-\ TcOX_4 \overset{-e}{\rightleftharpoons} [TcOX_4]^- \overset{+e}{\rightleftharpoons} [TcOX_4]^{2-} \qquad (3)$$
$$d^1\ (Br\ transient) \qquad d^2 \qquad d^3\ (expels\ X^-)$$

Electrolyte solutions of pentavalent $[TcOCl_4]^-$ and $[TcOBr_4]^-$ in CH_2Cl_2 are green and orange, respectively, even the bromo complex has no strong absorption features below 25 000 cm^{-1} [*cf.* Fig. 4(a) and 4(b)]. As we shall see, this in accord with their status as diamagnetic Tc^V ($4d^2$) centres containing a strongly perturbing O^{2-} ligand, with the first available metal acceptor level sufficiently raised in energy to shift XMCT well into the UV region. This formulation is also the basis for a sensible description of their voltammetric behaviour.

The UV/VIS spectra of $[NBu_4][TcOCl_4]$, $[NBu_4][TcOBr_4]$ and $TcOCl_4$ are summarised in Table 2. The *in situ* electrogeneration of $TcOCl_4$ was performed in the OTTLE cell in CH_2Cl_2 at 218 K. The initial spectrum of diamagnetic $[TcOCl_4]^-$ displays three broad absorptions, with the lowest-energy maximum near 28 000 cm^{-1}. This differs measurably from the spectrum of isoelectronic $[TcNCl_4]^{2-}$ which has no distinct bands below 35 000

Table 3 Optimised geometrical parameters (bond lengths in Å, angles in °) and energies* (eV) for $TcYX_4$ species (Y = N or O; X = Cl or Br)

Nitrido species				
	Tc–N	Tc–X	N–Tc–X	Energy
$[TcNCl_4]^{2-}$	1.640	2.387	105.0	−30.839
$[TcNCl_4]^{-}$	1.639 (1.581)	2.315 (2.322)	103.8 (103.3)	−32.060
$[TcNBr_4]^{2-}$	1.637	2.532	104.4	−28.883
$[TcNBr_4]^{-}$	1.640 (1.596)	2.461 (2.482)	103.8 (103.0)	−29.713
Oxo species				
	Tc–O	Tc–X	O–Tc–X	Energy
$[TcOCl_4]^{-}$	1.674 (1.593)	2.298 (2.309)	107.6 (106.8)	−30.790
$TcOCl_4$	1.674	2.253	106.1	−26.685
$[TcOBr_4]^{-}$	1.672 (1.613)	2.445 (2.460)	107.4 (106.6)	−28.463
$TcOBr_4$	1.678	2.402	105.8	−24.396

* Energies are relative to the energies of the component atoms calculated in their ground electronic state *via* spin-restricted calculations. Experimental data are included in parentheses where available.

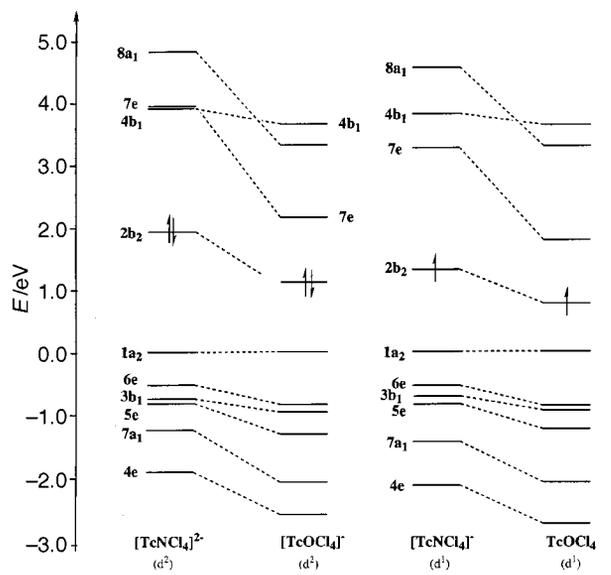

Fig. 5 Molecular orbital splitting diagram for $[TcNCl_4]^{-/2-}$ and $[TcOCl_4]^{0/-}$

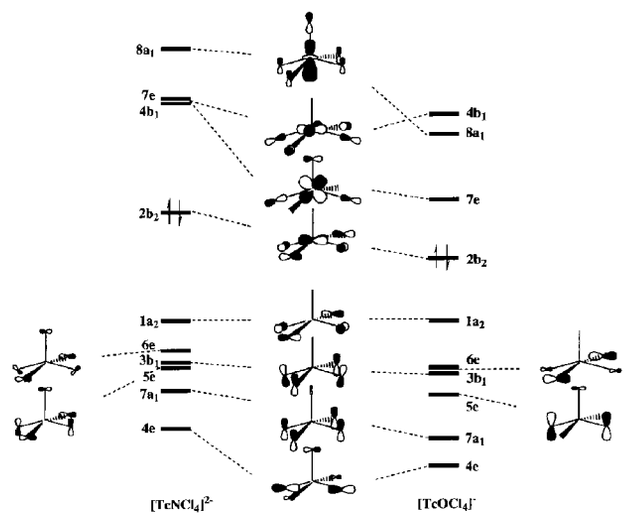

Fig. 6 Frontier molecular orbitals of $TcYX_4$ species (Y = N or O; X = Cl or Br). Energies as in Fig. 5, with $1a_1$ = zero

cm^{-1}. Electrogeneration at +2.4 V results in a colour change from green $[TcOCl_4]^-$ to purple $TcOCl_4$ and the growth of several new bands [Fig. 4(a)]. Despite the high generation potential, the purple colour of the Tc^{VI} species is retained under N_2 at 293 K for at least 24 h if light is excluded. However, repeated electrogeneration cycles between $TcOCl_4$ and $[TcOCl_4]^-$ can lead *via* oxidation of residual free Cl^- to Cl_2 to the formation of $[TcCl_6]^{2-}$ [see also caption of Fig. 4(a)]. In contrast, the irreversibility of the $[TcOBr_4]^{0/-}$ couple precluded the characterisation of $TcOBr_4$. Upon oxidation in CH_2Cl_2 in the OTTLE cell, the starting spectrum of orange $[TcOBr_4]^-$ shown in Fig. 4(b) collapses irreversibly, as expected from the voltammetry.

Computational results

Optimised geometries and calculated electronic structures. We have performed a series of density function calculations on d^1 and d^2 $\{TcYX_4\}$ complexes, in order to enhance our understanding of their electronic structures and relative redox potentials, and to assist the assignment of the UV/VIS spectra. Table 3 lists the computed energies for the eight species, together with the optimised geometries which were obtained assuming a C_{4v} square-pyramidal structure. Experimentally determined structural data for $[TcNX_4]^-$,[3,16] and for $[TcOX_4]^-$ (X = Cl or Br)[18,19] are included for comparison. The computed geometries are in good agreement with the experimental structures, with the Tc–X distance and Y–Tc–X angles being particularly well reproduced. The Tc–Y distances are slightly longer than those determined experimentally (by 3 to 4%), a consistent effect already noted[20] in a similar study of $[OsNCl_4]^-$, and in density functional calculations of related species.[2] Comparing the calculated d^1 and d^2 structures (Table 3), we find that reduction causes significant lengthening of the Tc–X bond, and a very slight expansion of the characteristic Y–Tc–X angle, but that the Tc–Y distance remains virtually unchanged. Similar computational results were obtained earlier for $[MoNCl_4]^-$ and $[MoNCl_4]^{2-}$, where comparison of known crystal structures for the d^0 and d^1 species supported the computed structural trend.[2] Finally, we note that the Tc–X bond is about 0.06–0.08 Å shorter in each oxo-species than in the isoelectronic nitrido analogue.

Molecular-orbital splitting diagrams for the four chloro complexes comparing the relative effects of the O^{2-} and N^{3-} ligands in the d^1 and d^2 pairs are shown in Fig. 5.‡ Fig. 6 shows a schematic representation of the frontier molecular orbitals of the d^2 $\{TcYCl_4\}$ species. The orbital arrangements shown in the centre of Fig. 6 are representative of all the $\{TcYX_4\}$ species discussed here. In contrast, the detailed nature of the e-symmetry halide-based orbitals (especially 5e and 6e) does alter significantly between the nitrido and oxo species, as indicated in the left- and right-hand side of Fig. 6. The HOMO of all these $\{TcYX_4\}$ species is a Tc–X π-antibonding $2b_2$ orbital lying in the pseudo-$\{TcX_4\}$ plane and is predominantly metal d_{xy} in

‡ The orbital numbering scheme used here differs from that employed elsewhere due to the inclusion of the sub-valence 4s and 4p electrons in our calculations. For example, the $7a_1$ and 6e orbitals in this work correspond to the $5a_1$ and 5e discussed by Deeth[21] and others.

character. The Tc^{V} d^2 complexes are therefore diamagnetic. To higher energy lie the remaining three Tc-based levels, $4b_1$, 7e, $8a_1$, having major contributions from the $d_{x^2-y^2}$, d_{xz}/d_{yz} and d_{z^2} orbitals, respectively, in antibonding combination with the appropriate ligand orbitals. Below these Tc-based orbitals are a cluster of predominantly halide-based non-bonding orbitals the nature of which will be discussed in more detail below. However, the highest lying, $1a_2$, is 100% chloride-based by symmetry and provides a convenient energy zero in Fig. 5 and Fig. 6, to which all the other levels have been referred. The absolute energy of this orbital will be affected nevertheless by coulombic effects and by the electron density prevailing at the metal (see below). To still lower energy and not shown in Figs. 5 and 6, are the Tc–ligand bonding orbitals, including $2b_1$ and $6a_1$ which (along with 4e) contribute strongly to Tc–X σ-bonding.

The different energetic splitting of the Tc-based orbitals in the d^2 oxo and nitrido species (*cf*. Fig. 6) obviously reflects the differing donor properties of the two axial ligands. Through its smaller nuclear charge, N^{3-} must be both a stronger σ- and π-donor than isoelectronic O^{2-}.[2] This stronger electronic donation by N^{3-} destabilises all the Tc-based orbitals in $[TcNCl_4]^{2-}$ relative to those of $[TcOCl_4]^{-}$. Thus, although there is no constructive overlap between the donor orbitals of the axial ligand and the in-plane Tc d_{xy} orbital ($2b_2$), the redox-active $2b_2$ HOMO of $[TcNCl_4]^{2-}$ is raised by 0.75 eV compared to its counterpart in $[TcOCl_4]^{-}$. This effect is augmented in the case of the $8a_1$ and 7e orbitals, which are directly Tc–Y σ- and π-antibonding respectively. In contrast, $4b_1$ (lying in the pseudo-TcX_4 plane, orthogonal to the axial ligand) is only 0.25 eV higher in $[TcNCl_4]^{2-}$ than in $[TcOCl_4]^{-}$, relative to non-bonding $1a_2$ in each case.

An explanation of the smaller displacement of $4b_1$ can be found in the detailed structures of the $TcYCl_4$ species. As noted above, the Tc–Cl bond is always shorter in the oxo-species compared to their isoelectronic nitrido analogues, which implies stronger Tc–Cl interaction in the oxo species. This is reflected in the energy of the strongly Tc–Cl σ-antibonding (but empty) $4b_1$ orbital, as depicted in the MO diagram of $[TcOCl_4]^{-}$. Increased electron density at the metal in isoelectronic $[TcNCl_4]^{2-}$ evidently weakens the Tc–Cl interaction. For $[TcOCl_4]^{-}$ the axial donation is not so strong and this is compensated by stronger Tc–Cl bonding in the $[TcOCl_4]^{-}$ species, resulting in a shorter Tc–Cl distance. This will also lead to closer Cl···Cl interatomic contacts, accounting for the wider spread of the occupied halide-based orbitals in the oxo species.

Comparative molecular orbital diagrams for d^1 $[TcNCl_4]^{-}$ and $TcOCl_4$ present a pattern similar to their d^2 analogues (*cf*. Fig. 5). Oxidation causes relative stabilization of the Tc-based orbitals, as expected. This stabilization is largest for the $2b_2$ and 7e orbitals (*ca*. 0.6 eV) but is small (<0.2 eV) for the $4b_1$ and $8a_1$ orbitals. Here the electrostatic effects of decreased electron-density are counter-balanced by stronger M–X bonding in Tc^{VI} *vs*. Tc^{V}. Similar changes are calculated between $[TcOCl_4]^{-}$ and $TcOCl_4$, although the effect is smaller (*ca*. 0.3 eV for $2b_2$ and 7e, and <0.05 eV for $4b_1$ and $8a_1$). These differential effects of the nitrido and oxo ligands have direct consequences for the UV/VIS spectra where these Tc-based orbitals play the role of acceptor orbitals in XMCT transitions.

The MO splitting diagrams computed for the $TcYBr_4$ systems are essentially equivalent to those described already, except that the non-bonding bromide levels are about 0.5 eV closer to the metal levels. This is a familiar consequence of the lower electronegativity of Br, and the higher energy of the 4s and 4p orbitals compared to their 3s and 3p Cl counterparts.

The nature of the singly occupied $2b_2$ orbital in $[TcNCl_4]^{-}$ has also been studied elsewhere by polarised neutron diffraction experiments supported by theoretical calculations, and this level was found to contain *ca*. 30% Cl character.[9,22] This resembles the 36% Cl character obtained here. Our calculation on $TcOCl_4$ bears instructive comparison with that reported by Deeth[21] for isoelectronic $[MoOCl_4]^{-}$. The main difference is the relative stabilisation of the metal-based orbitals (the calculated $1a_2 \longrightarrow 2b_2$ gap is only 0.8 eV for $TcOCl_4$ compared to 2.3 eV for $[MoOCl_4]^{-}$) and greater ligand character (= greater delocalisation) in the metal-based orbitals of $TcOCl_4$. Both results reflect the higher core-charge of Tc^{VI} compared to Mo^{V}. Several low-intensity bands occurring in the visible region of the spectrum of $[MoOCl_4]^{-}$ have been assigned to d–d bands or orbitally forbidden charge transfer processes.[23] In the case of $TcOCl_4$, the easier reduction of the metal centre means such features are largely obscured by the red-shifted intense charge-transfer processes into the low-lying metal acceptor orbital (see below).

Table 4 Calculated transition energies (cm^{-1}) for $[TcNX_4]^{-/2-}$ (X = Cl or Br)

Transition	$[TcNCl_4]^{2-}$	$[TcNCl_4]^{-}$	$[TcNBr_4]^{2-}$	$[TcNBr_4]^{-}$
Charge transfer processes				
$1a_2 \longrightarrow 2b_2$ *		14 000		9 000
$6e \longrightarrow 2b_2$		17 300		13 400
$3b_1 \longrightarrow 2b_2$ *		19 900		15 100
$5e \longrightarrow 2b_2$		20 100		15 770
$4e \longrightarrow 2b_2$		29 500		26 200
$1a_2 \longrightarrow 7e$	38 600	32 900	34 100	28 200
$6e \longrightarrow 7e$	38 600	34 600	36 100	31 600
$3b_1 \longrightarrow 7e$	43 700	38 200	39 300	33 700
$5e \longrightarrow 7e$	43 700	38 700	39 400	34 500
$7a_1 \longrightarrow 7e$	42 700	39 600	40 600	37 200
$4e \longrightarrow 7e$	49 700	47 400	47 100	44 500
$6e \longrightarrow 4b_1$	37 600	35 200	32 500	29 600
$5e \longrightarrow 4b_1$	40 700	37 900	34 700	31 900
$3b_1 \longrightarrow 4b_1$	41 000	37 500	34 700	31 100
d–d Transitions				
$2b_2 \longrightarrow 7e$	17 600	22 600	17 900	22 600
$2b_2 \longrightarrow 4b_1$	14 500	21 800	13 200	20 100
$2b_2 \longrightarrow 8a_1$	25 500	32 800	26 000	31 500

* Orbitally-forbidden process.

Calculated charge-transfer energies. The intensities of the major bands ($\varepsilon > 1000$ dm^3 mol^{-1} cm^{-1}) in the spectra of d^1 and d^2 $TcYX_4$ species are consistent with their assignment as charge-transfer processes. As the highest occupied ligand orbitals are predominantly halide-based, excitation from these orbitals into one of the vacant Tc-based orbitals are properly classified as halide-to-metal charge transfer (XMCT). Accordingly, we have calculated energies for all spin- and orbitally-allowed XMCT transitions that occur within the spectroscopically accessible range. For C_{4v} symmetry, all transitions involving an e-type orbital are orbitally-allowed, as are transitions between two orbitals of the same symmetry. The calculated XMCT energies are listed in Table 4 for d^1 and d^2 $TcNX_4$ and in Table 5 for $[TcOX_4]^{-}$ and $TcOCl_4$ with the energies calculated for d–d transitions and selected orbitally-forbidden processes also included.

Composition of halide-based donor orbitals. In addition to transition energies and the symmetry constraints described above, the intensities of each transition must also be considered. Oscillator strengths of XMCT bands are known to be related to the relative orientations of the halide donor and metal acceptor orbitals involved in the transition.[24] Detailed analysis indicates that the significant contribution to XMCT intensities is derived from the presence of similarly orientated *halide* character in both the donor and acceptor orbitals.[25,26]

Unfortunately, we are unable to compute oscillator strengths directly in this present work. However the relative orientations of the orbitals involved provide a qualitative idea of the likely transition intensities. Fig. 7 shows how the halide symmetry orbitals of a planar $\{X_4\}^{4-}$ array arise from the various com-

Table 5 Calculated transition energies (cm^{-1}) for $[TcOX_4]^{0/-}$ (X = Cl or Br)

Transition	$[TcOCl_4]^-$	$TcOCl_4$	$[TcOBr_4]^-$
Charge transfer processes			
$1a_2 \longrightarrow 2b_2$*		8 800	
$6e \longrightarrow 2b_2$		15 600	
$3b_1 \longrightarrow 2b_2$*		15 900	
$5e \longrightarrow 2b_2$		18 700	
$4e \longrightarrow 2b_2$		29 200	
$1a_2 \longrightarrow 7e$	22 400	18 700	17 700
$6e \longrightarrow 7e$	27 800	24 700	23 500
$3b_1 \longrightarrow 7e$	28 500	25 200	24 200
$5e \longrightarrow 7e$	31 300	27 400	27 300
$7a_1 \longrightarrow 7e$	36 500	33 500	32 600
$4e \longrightarrow 7e$	40 100	38 300	37 100
$6e \longrightarrow 4b_1$	37 900	36 200	31 600
$5e \longrightarrow 4b_1$	41 700	38 400	35 700
$3b_1 \longrightarrow 4b_1$	38 900	36 900	32 500
$6e \longrightarrow 8a_1$	35 900	35 320	
$5e \longrightarrow 8a_1$	39 300	38 540	
$7a_1 \longrightarrow 8a_1$	44 700	44 300	
d–d Transitions			
$2b_2 \longrightarrow 7e$	9 300	13 200	9 608
$2b_2 \longrightarrow 4b_1$	18 600	24 400	17 100
$2b_2 \longrightarrow 8a_1$	19 200	25 100	18 800

* Orbitally-forbidden process.

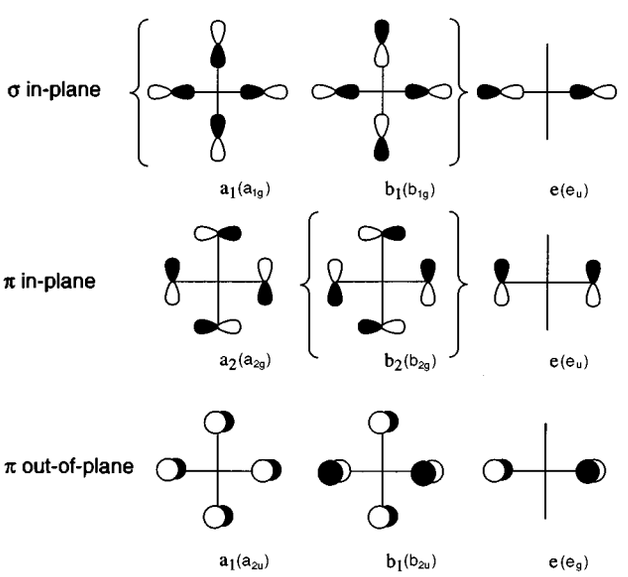

Fig. 7 Halide p-orbital combinations associated with the planar $\{X_4\}^{4-}$ array in a pyramidal C_{4v} environment (D_{4h} labels added)

binations of twelve halide p orbitals.[6] We use C_{4v} symmetry labels to identify the orbitals characterising the $\{X_4\}^{4-}$ array for ease of comparison with the present $\{MYX_4\}$ analysis; the higher-symmetry D_{4h} labels given in parentheses. For the five-co-ordinate Tc complexes under study, three of these orbitals (those contained in braces in Fig. 7) are strongly stabilised by their bonding interaction with the metal orbitals, and do not figure in subsequent discussion. The six remaining available levels (counting each e-pair only once) form the basis of the series of occupied halide-based orbitals shown in Fig. 6. This manifold features two in-plane π-orbitals (a_2 and e), one in-plane σ-orbital (e) and three out-of-plane π-orbitals (a_1, b_1 and e). Although the out-of-plane π e-pair appears to have the correct orientation to interact with the Tc e orbitals (d_{xz}/d_{yz}), this interaction is small, due to both the Y–Tc–X angle, which reduces overlap between these two orbitals, and to the much stronger interaction of the empty metal e-level with the e-type donor orbitals of the axial ligand, Y.

Table 6 Calculated major orbital percentage contributions to e-type donor orbitals in d^1 $[TcYX_4]$ species (Y = N, X = Cl or Br; Y = O, X = Cl)

		6e	5e	4e
$[TcNCl_4]^-$	σ-in-plane	16.0	2.5	57.4
	π-in-plane	38.7	44.2	14.3
	π-out-of-plane	32.8	46.0	16.8
	axial	11.6	5.0	10.9
$[TcNBr_4]^-$	σ-in-plane	17.1	0.9	62.2
	π-in-plane	55.5	27.1	15.1
	π-out-of-plane	20.7	64.5	6.4
	axial	6.5	5.2	9.9
$TcOCl_4$	σ-in-plane	12.1	0.1	58.0
	π-in-plane	82.6	2.1	13.2
	π-out-of-plane	0.8	86.9	3.0
	axial	3.3	0.0*	18.4

* 10% Metal character.

The composition of the non-bonding halide orbitals in the $TcYX_4$ species derived from this picture may be complicated, by mixing of axial ligand character and/or by mixing between the three halide-based e orbitals. The extent of these effects is detailed in Table 6 for the d^1 species (similar orbital characteristics are computed for the halide-based e-levels of the d^2 species). The calculations indicate that the degree of axial ligand character involved in these orbitals is rather small. However, the in-plane/out-of-plane mixing within e-symmetry differs greatly from one species to another. For $TcOCl_4$ little mixing occurs, and the three e-type donor levels remain relatively pure in terms of their spatial orientation, *i.e.* σ-in-plane, π-out-of-plane and π-in-plane for 4e, 5e and 6e respectively (*cf.* Table 6 and Fig. 6). This is *not* the case for the nitrido species, in which considerable mixing of in- and out-of-plane π-character appears to be induced by the presence of the N^{3-} ligand. Such variations in the physical nature of the halide donor orbitals will be important in assigning the UV/VIS spectra of these systems.

Discussion

Trends in redox potentials

We have recently compared the d^0/d^1 couples of octahedral $MoCl_6$, pseudo-octahedral $[MoOCl_5]^-$ and square-pyramidal $[MoNCl_4]^-$.[2] It was found that the substantial changes in redox potentials in these complexes were linked to the extent of negative-charge donation by the axial ligands. This capability (and hence the stabilisation of the higher metal oxidation state) increases, as the axial ligands vary, in the order $\{Cl\cdots Cl\}^{2-} < \{O\cdots Cl\}^{3-} < N^{3-}$. For the present Tc systems, the larger interaction of the nitrido ligand compared to the oxo ligand is evident in the calculated MO splitting diagrams (Fig. 5). Relative to the non-bonding $1a_2$ orbital, the $2b_2$ HOMO is destabilised by 0.75 eV for $[TcNCl_4]^{2-}$ with respect to $[TcOCl_4]^-$. In other words, axial destabilisation is greater for N^{3-} than O^{2-} and so the $d^2 \longrightarrow d^1$ oxidation, which removes an electron from the b_2 orbital is more facile for $[TcNCl_4]^{2-}$ than $[TcOCl_4]^-$. Indeed a subsequent $d^1 \longrightarrow d^0$ oxidation is observed for $[TcNCl_4]^-$, while the equivalent process is not accessible for $TcOCl_4$.

Fig. 5 makes clear that the effect of the strong Tc–N interaction is even more marked in destabilising the unoccupied d-orbitals, in particular the 7e and $8a_1$ orbitals which are directly Tc–N antibonding. As a consequence, no further reduction of $[TcNCl_4]^{2-}$ (which would require population of the 7e orbital) is observed within the solvent range. In contrast, although irreversible, the $d^2 \longrightarrow d^3$ reduction of $[TcOCl_4]^-$ is observed at a relatively accessible potential.

It is notable that the redox potential for $[TcNCl_4]^{-/2-}$ is very similar to that reported for the isovalent $[MoNCl_4]^{-/2-}$ couple (see Table 1), despite the unit increase in elemental atomic

number (which assists reduction through core-charge effects). The reason lies in the enforced spin pairing in the energetically isolated b_2 orbital for d^2 $[TcNX_4]^{2-}$, and the resultant loss of exchange energy; this makes addition of one electron much more difficult than would otherwise be expected for Tc^{VI}. For the parent hexahalide complexes, in contrast, the isovalent VI/V couples are as follows, for $[MoCl_6]^{0/-}$ (d^0/d^1), $E_{\frac{1}{2}} = +2.2$ V, and for $[TcCl_6]^{0/-}$ (d^1/d^2), $E_{\frac{1}{2}} = +3.2$ V (estimated).[27] This shift of *ca.* 1 V in potential between the neighbouring $[MoCl_6]^{0/-}$ and $[TcCl_6]^{0/-}$ couples reflects the normally dominant role of the metal core charge. In the MX_6 $4d^n$ complexes, the deviation in $E_{\frac{1}{2}}$ values due to spin-pairing is of course observed for the d^3/d^4 couple. Thus, the $[TcCl_6]^{2-/3-}$ (d^3/d^4) couple is almost coincident with $[MoCl_6]^{2-/3-}$ (d^2/d^3) despite technetium's greater core charge.[10,11] Turning to the oxo-analogues, the d^0/d^1 $[MoOCl_5]^{-/2-}$ couple occurs at +1.70 V, while the d^1/d^2 $[TcOCl_4]^{0/-}$ couple is observed here at $E_{\frac{1}{2}} = +1.84$ V. Both experimental and theoretical evidence suggests that the effect of the axial fifth chloride ligand on the Mo couple is small. The calculated electron affinity of $[MoNCl_4]^-$ is −1.22 eV[2] while the energies quoted in Table 3 lead to the same value (−1.22 eV) for the electron affinity of $[TcNCl_4]^-$. Our analogous calculations§ on $MoOCl_4$ and $[MoOCl_4]^-$ give an electron affinity of 4.04 eV for $MoOCl_4$ compared to 4.11 eV calculated here for $TcOCl_4$. For the $Tc^{V/IV}$ couples, we find the corresponding experimental electrode potentials take the values +1.95 V for $[TcCl_6]^{-/2-}$ [28] and −0.52 V for $[TcOCl_4]^{-/2-}$, with the corresponding $[TcNCl_4]^{2-/3-}$ unobserved but presumably well beyond −2.6 V. These observations illustrate that the pattern of redox data for isovalent series of analogous metal complexes is crucially dependent on the splitting and occupancy of the metal d orbitals and therefore on the co-ordination environment (including geometry and ligand identity).

The measured redox potentials of the $TcYBr_4$ species are similar to their chloro analogues, as commonly observed in $4d^n$ and $5d^n$ halide complexes.[5,29] From an electronic structural viewpoint, the same degree of Tc–X mixing is calculated in the metal-based orbitals, despite the bromide donor orbitals lying at higher energy than their chloride counterparts. It seems the smaller energy mismatch between the Tc 4d and Br donor orbitals is offset by the intrinsically greater Tc–Br internuclear separation which reduces the metal–halide overlap. Overall, the condition of the metal centre appears similar in analogous chloride and bromide complexes.

General trends in optical spectra

It is noteworthy that $Tc^{VI}N$ complexes which lack co-ordinated halide, such as $[TcN(H_2PO_4)_4]^-$ and $[TcN(HSO_4)_4]^-$, give colourless solutions and show no intense absorbances below 30 000 cm^{-1}.[30] In contrast the UV/VIS spectra of the $\{TcYX_4\}$ species examined here are dominated, as expected, by halide-to-metal charge transfer 'XMCT' bands. However in some respects these spectra are surprising. For this reason, it is helpful to review the distinguishing characteristics of familiar systems containing a planar $\{MX_4\}$ chromophore. Low-spin d^5 complexes such as D_{4h} *trans*-$[RuX_4(MeCN)_2]^-$ or C_{4v} *trans*-$[OsX_4(CO)(MeCN)]^-$ (X = Cl or Br)[5,6,31] are analogous to the present d^1 Tc species in that they possess a singly occupied metal-based acceptor orbital (d_{xy}) lying in the $\{MX_4\}$ plane, and they display an unmistakable spectral signature in the form of an intense charge-transfer doublet as explained below. Group theory predicts only two allowed XMCT transitions from several distinct ligand levels of Fig. 7; *viz.* $2 \times e_u \longrightarrow b_{2g}$, assuming local D_{4h} symmetry. Formally forbidden promotion from a_{2u} or b_{2u} represents excitation from an *out-of-plane* (or 'vertical') halide symmetry orbital to the in-plane dπ metal acceptor orbital; this is a relatively unfavoured process (as explained in the next section) and such bands are not observed. In contrast, the two sets of ligand-centred e_u symmetry orbitals do lie in the *xy* plane; though formally subject to mixing they have essentially different origins, in-plane Xπ which is uppermost in energy and in-plane Xσ which is more stabilised (*cf.* Fig. 7).

Accordingly, two XMCT manifolds are observed in the spectra of such d^5 *trans*-MX_4L_2 species, a prominent visible band due to in-plane $X(\pi/\sigma) \longrightarrow M(d\pi)$, and a less intense band attributable to in-plane $X(\sigma/\pi) \longrightarrow M(d\pi)$ lying some 10 000 to 15 000 cm^{-1} higher in energy (*i.e.* well into the UV region). Since there is the possibility of symmetry-mixing between the two e_u levels, the π/σ notation is employed to indicate predominant π character. The orbital degeneracy of the halide e_u levels means that the CT excited state is subject to *ligand*-centred spin–orbit coupling which causes distinctive band splitting of 700–900 cm^{-1} for MCl_4 centres (not always resolved), expanding to 2000–2500 cm^{-1} in their MBr_4 counterparts.[5] Another diagnostic characteristic of these systems[5] is that when Br replaces Cl, the centre of gravity of the leading doublet [due to $X(\pi/\sigma) \longrightarrow M(d\pi)$ excitation] shifts by about 6000 cm^{-1}, in accord with their standard optical electronegativities.[32] A weak but characteristic satellite band is seen on the red edge of the principal $X(\pi/\sigma) \longrightarrow M(d\pi)$ doublet band in *trans*-$[RuX_4(MeCN)_2]^-$ and related complexes; this has been assigned to the in-plane but symmetry-forbidden XMCT excitation, $a_{2g} \longrightarrow b_{2g}$. When d^1 $[TcNCl_4]^-$ and $[TcNBr_4]^-$ are dissolved in aqueous HCl or HBr,[1] XMCT spectra unmistakably resembling the MX_4 archetype are observed. It is impressive to realise that in this case as well, albeit for very different reasons, the only readily accessible metal-acceptor level is the singly occupied d_{xy} orbital.

Remarkably enough, spectral profiles very similar to those described above are also observed for the XMCT manifold of metal–metal bonded $[M_2X_8]^{z-}$ complexes (M = Tc or Re; X = Cl, Br or I; $z = 2$ or 3), dictated by the presence of the $\{MX_4\}$ chromophore. The M–M δ* molecular orbital (locally akin to d_{xy}) is the metal-based acceptor orbital in this case.[33] Despite the presence of the M–M triple bond and the departure from planarity within the MX_4 moiety, the same unmistakable XMCT envelope is observed for these binuclear species. These well-behaved $M_2X_8^{z-}$ examples are introduced particularly because $[Tc_2X_8]^{2-}$ and $TcYX_4$ share a very similar pyramidal displacement of the metal above the $\{X_4\}$ plane, with experimentally determined Tc–Tc–X and N–Tc–X angles of 104 and 103° respectively.

The visible spectra of $[TcNX_4]^-$ dissolved in *ca.* 7 M HX resemble those anticipated for a normal $\{MX_4\}$ chromophore, and this circumstance justifies the attention devoted to such species above. However the spectra of the nitrido complexes dissolved in MeCN or CH_2Cl_2, or in the CH_2Cl_2–0.5 M NBu_4BF_4 electrolyte, show further complexities that are obvious in Fig. 2. Comparative solution studies[34] demonstrate that axial solvation or anation is definitely *not* responsible for the additional bands encountered in these media. Thus, $[TcNX_4]^-$ spectra in butan-2-one are similar to those in MeCN, but progressive addition of co-ordinating dioxane *simplifies* the spectrum until the 'typical $\{MX_4\}$ profile' is achieved.[34] In summary, the species in HX_{aq} is now thought to be $[TcNX_4(H_2O)]^-$ and it appears that axial solvation or anation is responsible for the simplification of the spectra in such solvents (rather than the reverse!). This confirms our conclusions based on the present reflectance measurements on powdered samples of $[NBu_4]$-$[TcNX_4]$ (X = Cl or Br), where the five-co-ordinate nature of the metal centre in the crystal lattice is certain. The solid-state spectra (5000 to 35 000 cm^{-1}) correspond in detail with the Tc^{VI} spectra presented in Fig. 2(a) and 2(b), as evident from Table 2.

The general account of $\{MX_4\}$ chromophores[6] outlined above gives no indication of how such unforeseen complexities could arise for $[TcNCl_4]^-$, especially when not observed for

§ Optimised parameters for $MoOCl_4$: Mo–O 1.691, Mo–Cl 2.276 Å; O–Mo–Cl 103.9°; for $[MoOCl_4]^-$: Mo–O 1.699, Mo–Cl 2.329 Å; O–Mo–Cl 105.8°.

isostructural $TcOCl_4$. Indeed, initially these spectra seemed challenging enough to undermine the basis of the previous, intuitively simple view of such chromophores. In the following discussion, the density functional calculations are employed to investigate and resolve this intriguing problem.

There is also a more straightforward distinction between the d^5 species considered earlier and the present d^1 or d^2 Tc systems, namely that, at least in principle, excitations to the vacant, higher-lying d orbitals (d_{xz}/d_{yz} = 7e) should also be observed. This is particularly clear in the spectra of $[TcOX_4]^-$ (see below), and helps to map the energetic relationship between the various dπ levels (assuming reliable assignments can be made).

The nitrido complexes

(i) $[TcNCl_4]^{2-}$ and $[TcNCl_4]^-$. The spectrum of electrogenerated d^2 $[TcNCl_4]^{2-}$ shows no strong absorption below 35 000 cm^{-1}. The absence of low-energy CT bands reflects the lack of a low-lying acceptor orbital, due to the double occupancy of the $2b_2$ orbital and the extremely strong Tc–N interaction which destabilises all the metal acceptor levels, but especially 7e. In $[TcNCl_4]^{2-}$ this reaches the point that π-destabilised 7e is accidently degenerate with σ-antibonding $4b_1$ ($d_{x^2-y^2}$). (Although these approximate descriptions are helpful, strict differentiation between σ- and π-type M–L bonding is lost in the heavily pyramidal C_{4v} MYX_4 framework.) The first XMCT transition is calculated to be $6e \longrightarrow 4b_1$ at 37 600 cm^{-1}, although several other promotions involving both 7e and $4b_1$ as acceptor orbitals are predicted to lie nearby.

Regeneration of $[TcNCl_4]^-$ [as in Fig. 2(a)] sees the recovery of the three characteristic bands at 21 900, 24 580 and 33 340 cm^{-1}. All of these bands are likely to arise from promotions to the now singly-occupied $2b_2$ orbital. Symmetry and energy considerations jointly suggest these transitions are most likely to involve promotion from an e-type ligand level, of which there are three, and this is also consistent with the doublet structure of the band centred at 21 900 cm^{-1}. However, the presence of three bands for $[TcNCl_4]^-$ in CH_2Cl_2 solution stands in contrast to the behaviour of typical MX_4L_2 chromophores which exhibit only two strong XMCT bands some 10 000 cm^{-1} or more apart, as noted above.

In general terms, for a transition to the in-plane $2b_2$ (dπ) acceptor orbital to have significant intensity, the donor orbital must also exhibit significant in-plane π-character. In other words, the requirement is for commonality of bonding character, as well as halide admixture in the acceptor orbital. Table 6 indicates that a substantial (and quite exceptional) degree of mixing of in-plane and out-of-plane (= 'vertical') π character occurs in the e-type donor levels in $[TcNCl_4]^-$. As a result *all three* e-type donor orbitals have significant in-plane π character and promotions from all three to the $2b_2$ acceptor orbital are observed. The energies of these transitions are calculated at 17 300, 20 100 and 29 500 cm^{-1}, for the 6e, 5e and 4e donor levels, respectively, consistently about 4000 cm^{-1} lower than the observed bands. A similar, roughly uniform under-estimation of the energies of XMCT processes by density-functional methods has been noted before, in SCF-Xα calculations.[27] It is encouraging that the $e \longrightarrow 2b_2$ computations correctly reproduce the splitting of the three absorptions. We conclude the observed bands at 21 900 and 24 580 cm^{-1} can both be assigned to in-plane Cl (**π**/σ) ⟶ Tc (dπ) promotions, and the one at 33 340 cm^{-1} assigned to in-plane Cl (**σ**/π) ⟶ Tc (dπ).

Two weak features remained to be assigned in the visible spectrum of $[TcNCl_4]^-$: the band at 19 100 cm^{-1} and the shoulder at 20 900 cm^{-1}. These bands only appear in the spectrum of the oxidised species and probably arise from symmetry-forbidden processes involving the $2b_2$ acceptor orbital. Two possibilities are $1a_2 \longrightarrow 2b_2$, corresponding to the $1a_{2g} \longrightarrow 2b_{2g}$ transition proposed for $[MX_4L_2]^-$ species, and $3b_1 \longrightarrow 2b_2$, as already identified for related $[MoOCl_4]^-$ and $[MoOCl_4(H_2O)]^-$.[21,23]

The general stabilisation of the Tc-based orbitals upon oxidation means that the transitions to the upper-storey 7e and $4b_1$ orbitals for $[TcNCl_4]^{2-}$ are calculated to be red-shifted by between 2300 and 5700 cm^{-1} in $[TcNCl_4]^-$. The shift to lower energy of the intense UV absorption edge [Fig. 2(a)] seems to be of about this magnitude, so promotions to these levels probably account for the broad new absorption maximum at 43 000 cm^{-1} in $[TcNCl_4]^-$. Definitive assignments in this region are hampered by the proximity of a number of allowed transitions, and by uncertainties over whether or not a systematic adjustment of *ca.* 4000–5000 cm^{-1} can be applied legitimately to all the calculated CT energies. For $[TcNCl_4]^-$, without being prescriptive, we note that among the seven contending transitions in Table 4 with *calculated* energies between 34 000 and 40 000 cm^{-1}, $3b_1 \longrightarrow 4b_1$, and especially $6e \longrightarrow 4b_1$ are eminently suited in terms of donor/acceptor-level compatibility to contribute to the intense higher-frequency UV bands. If this is the case, the intensity of the 43 000 cm^{-1} maximum owes a lot to the element of Xσ–Mσ character, which is a familiar finding for similar bands in other halide complexes.[26] On the other hand, in $[TcNCl_4]^-$, the composition of 7e reflects far more Tc–N interaction than Tc–Cl_4 interaction (46% d_{xz},d_{yz} and 42% axial N π-character *vs.* 8% net Cl in-plane π-character; *cf.* Fig. 6) suggesting this acceptor level is distinctly less well-suited to XMCT.

(ii) $[TcNBr_4]^{2-}$ and $[TcNBr_4]^-$. Like $[TcNCl_4]^{2-}$ (discussed above), and for the same reasons, electrogenerated $[TcNBr_4]^{2-}$ is notable in having no intense absorptions below about 35 000 cm^{-1}. This is quite remarkable for a high-valent metal bromide and reflects the extreme axial perturbation of the parent octahedral t_{2g} orbitals by the axial N^{3-} ligand, sufficient to impose a low-spin d^2 configuration on the complex.

The regeneration of $[TcNBr_4]^-$ is shown in Fig. 2(b). Considering first the higher UV region, we note the red-shift of the intense absorption upon oxidation brings two intense maxima into the accessible range, at 34 000 and 37 000 cm^{-1}. Among many possibilities, $3b_1 \longrightarrow 4b_1$ and $6e \longrightarrow 4b_1$ stand out as strong contenders to contribute to these bands (Table 4) exactly as for $[TcNCl_4]^-$, with $6e \longrightarrow 7e$ the most likely means of achieving CT to 7e although this promotion appears physically less favoured than the transitions to $4b_1$.

On first inspection, the visible manifold of d^1 $[TcNBr_4]^-$ appears to contain three strong maxima, instead of the single well-spaced doublet expected for a simple MX_4 chromophore. It is helpful to explain immediately that the manifold actually contains four components in the form of *two* spin–orbit doublets that straddle one another. Further solution studies on $[TcNBr_4]^-$ confirm that this envelope should be interpreted as two overlapping spin–orbit doublets (with components at 16 300/19 200 and 17 900/19 600 cm^{-1}) centred at 17 800 and 18 800 cm^{-1} respectively.[34] Thus, $[TcNBr_4]^-$ actually corresponds closely with its chloro analogue by having two $e \longrightarrow b_2$ X(π/σ) ⟶ Tc (dπ) transitions in this spectral region. Examined more critically, the two complexes differ in the sense that the lower-energy doublet (comprising the first and third components) is the more intense of the two for the bromide, while the reverse is true for $[TcNCl_4]^-$. In addition, $[TcNBr_4]^-$ reveals a broad doublet shoulder centred at 29 000 cm^{-1} which may correspond to the band above 33 000 cm^{-1} in $[TcNCl_4]^-$. The bathochromic shift between $[TcNBr_4]^-$ and its chloro analogue is fairly consistent at 4000 to 6000 cm^{-1} for these three spectral features, assuming the correct correlations have been drawn.

The experimental bathochromic shift of the XMCT bands in the spectrum of $[TcNBr_4]^-$ is reproduced by the trend in calculated energies for the three $e \longrightarrow b_2$ type transitions, which have much the same mutual separations as those derived for $[TcNCl_4]^-$. The multiple absorptions between 15 000 and 21 000 cm^{-1} are then assigned to two in-plane XMCT pro-

cesses, $6e \longrightarrow 2b_2$ and $5e \longrightarrow 2b_2$ (E_{calc} = 13 400 and 15 700 cm^{-1} respectively; shifted by some 4000 cm^{-1} from their calculated chloro-counterparts). It was noted above that the relative intensities of the bands associated with the 5e and $6e \longrightarrow 2b_2$ manifolds have changed compared to those observed for the chloride. We find that this is reflected in the calculated decrease in the in-plane π-character of the 5e orbital for $[TcNBr_4]^-$ *vs.* $[TcNCl_4]^-$ (27 *vs.* 39%) and the coupled increase of in-plane π-character for the 6e orbital (56 *vs.* 44%), *cf.* Table 6. Perhaps more dramatic is the observation that in 'well-behaved' $TcOCl_4$ (see below) the corresponding figure for in-plane π-character is 2% for 5e and 83% for 6e, so that in this isostructural complex all the intensity resides in the one $6e \longrightarrow 2b_2$ in-plane promotion.

By analogy with $[TcNCl_4]^-$, a third in-plane XMCT band rich in σ-character ($4e \longrightarrow 2b_2$, E_{calc} = 26 200 cm^{-1}) is anticipated. This corresponds well to the double shoulder in the bromide spectrum at 28 500 and 30 000 cm^{-1}. Another clearly-defined band is observed nearby, at 24 400 cm^{-1}, but given that our computed energies seem consistently lower than the observed energies, it would be difficult to justify transferring the very reasonable $4e \longrightarrow 2b_2$ assignment given above. At present, we do not have a definite explanation for this minor but interesting feature. Finally, the weak band at 13 000 cm^{-1} can be assigned to the orbitally forbidden in-plane $1a_2 \longrightarrow 2b_2$ XMCT transition (equivalent to the 19 000 cm^{-1} band for the chloride).

(iii) Spectra of $[TcNX_4]^-$ in concentrated aqueous acid. As mentioned above, the species formed in 7.5 M aqueous HX is believed to be $[TcNX_4(H_2O)]^-$ (where X = Cl or Br). The spectra of these two solvated species are characterised by a loss of intensity of the 'extra' $X(\pi/\sigma) \longrightarrow Tc(d\pi)$ band, which corresponds to the $6e \longrightarrow 2b_2$ transition of the unsolvated species. Preliminary calculations on $[TcNCl_4(H_2O)]^-$ support this idea. The C_{2v} symmetry of this molecule results in the e-type levels being split into b_1 and b_2 contributions and also removes the possibility of numerically partitioning in-plane σ and π character in our computational analysis. However the average *total* in-plane character of the $6b_1/6b_2$ (≈5e) and $7b_1/7b_2$ (≈6e) pairs of $[TcNCl_4(H_2O)]^-$ are calculated to be 71 and 25%, respectively. The equivalent orbitals in C_{4v} $[TcNCl_4]^-$ exhibit 47 (5e) and 55% (6e) total in-plane character, most of which is in-plane π (5e/39%, 6e/44%). This demonstrates a marked reduction of in-plane π-character in the $7b_1/7b_2$ (≈6e) orbitals upon formation of the adduct, consistent with loss of absorption in the region where the 'extra' $Cl(\pi/\sigma) \longrightarrow Tc(d\pi)$ band is found for five-co-ordinate $[TcNCl_4]^-$. A weak band is observed at 20 800 cm^{-1} in the aquated species. This might be a remnant of the lower-energy $Cl(\pi/\sigma) \longrightarrow Tc(d\pi)$ transition just discussed ($6e \longrightarrow 2b_2$), or a spin-forbidden process equivalent to the $a_{2g} \longrightarrow b_{2g}$ excitation described earlier. A similar weak feature in the spectrum of $[MoOCl_4(H_2O)]^-$ has been assigned to the $3b_1 \longrightarrow 2b_2$ transition, in accord with MCD evidence which was unequivocal in that instance,[23] but that assignment does not seem to suit the $[TcNX_4]^-$ species in energetic terms.

The oxo complexes

$[TcOCl_4]^-$ and $[TcOBr_4]^-$. It is noticeable in Fig. 3 (and Table 2) that the oxotechnetium(V) complexes $[TcOCl_4]^-$ and $[TcOBr_4]^-$ possess a strong well-defined band in the midst of the UV region (at *ca.* 33 000 and 28 000 cm^{-1} respectively), in contrast to their nitrido-analogues. As shown in Fig. 5, replacing N by O is computed to lower the 7e level selectively. The low-spin d^2 configuration is retained although the calculated splitting between the $2b_2$ and 7e levels in $[TcOCl_4]^-$ diminishes to 'only' 8000 cm^{-1} compared to the enormous 20 000 cm^{-1} $2b_2$/7e splitting encountered in $[TcNCl_4]^-$. Accordingly, the 7e level becomes accessible to XMCT processes in $[TcOX_4]^-$ complexes at frequencies within the normal spectral range. The next acceptor orbital in $[TcOCl_4]^-$ ($8a_1$) is computed to lie nearly 10 000 cm^{-1} above 7e. These considerations mean that the 33 000 cm^{-1} band in the spectrum of $[TcOCl_4]^-$ (and its partner in $[TcOBr_4]^-$) can be confidently attributed to XMCT processes involving the 7e acceptor level.

More detailed assignment of this absorption is problematic. Transitions from all six Cl-based orbitals to 7e (*cf.* Table 5) are allowed by symmetry. One of these, $4e \longrightarrow 7e$, can certainly be ruled out for energetic reasons (E_{calc} = 40 100 cm^{-1}); likewise $7a_1 \longrightarrow 7e$ is probably already too high in energy to explain the 33 300 cm^{-1} band (E_{calc} = 36 500 cm^{-1}), given the tendency for under-estimation in the calculations. Examining the nature of the computed 7e level more closely, one notes that while the metal character is predominantly out-of-plane π (*ca.* 55% Tc, d_{xz}/d_{yz}) the major contribution from the four halide ligands has in-plane σ-character (17%), with, perhaps unexpectedly, *less than 2% vertical halide π character*. Given that the presence of similarly oriented halide character in both donor and acceptor orbitals is paramount in determining XMCT intensities, the donor levels with significant in-plane σ-character deserve most attention. This clearly discounts excitation from the $1a_2$ donor orbital (100% π) as the source of an intense transition, and 5e likewise (<1% in-plane σ, 2% in-plane π, 90% out-of-plane π). The make-up of the three remaining donor levels is as follows, 6e (13% in-plane σ, 83% in-plane π), $3b_1$ (20% in-plane σ, 75% out-of-plane π) and $7a_1$ (10% in-plane σ, 75% out-of-plane π, but probably too energetic for this region) suggests that 6e and especially $3b_1$ are most likely to be implicated in the observed spectrum. The corresponding levels in $[TcOBr_4]^-$ have very similar compositions (within 1%) to those described for $[TcOCl_4]^-$. Finally, we note that the $3b_1 \longrightarrow 7e$ promotion is *xy*-polarised, with a tendency to shift electronic charge within the MX_4 pseudo-plane, whereas $6e \longrightarrow 7e$ is *z*-polarised and likely to be intrinsically weaker in terms of XMCT. Direct computation of oscillator strengths would clearly be of help in this regard. It is worth stressing how the calculated make-up of 7e in the oxo complexes is significantly different from the situation in the nitrido system, discussed above, where 7e embodies a major contribution from the axial ligand and is ill-suited to halide-to-metal CT processes. A weaker but distinct band at 28 000 cm^{-1} might be considered to be $6e \longrightarrow 7e$, which would require E_{calc} to coincide with E_{hv} for this transition.

Similar issues are involved in the assignment of the intense higher energy band, located at 42 200 cm^{-1} in $[TcOCl_4]^-$ and 39 800 cm^{-1} in $[TcOBr_4]^-$. For $[TcOCl_4]^-$, considering in turn the six transitions in Table 5 with E_{calc} in the range 36 to 40 kK (to allow for the probable underestimation by 2000 to 5000 cm^{-1}), we have $7a_1$,$4e \longrightarrow 7e$ [though *z*-polarised e/e XMCT excitations can be relatively unpromising, as noted above]; 6e,$3b_1 \longrightarrow 4b_1$ [both promising]; 5e,$6e \longrightarrow 8a_1$ [$6e \longrightarrow 8a_1$ can be dismissed through zero orbital compatibility]. Similarly, $5e \longrightarrow 8a_1$ depends on the mutual vertical halide character of donor and acceptor (90 and 17% respectively), but this vertical character is seen to switch abruptly from strongly Xπ (5e) to Xσ ($8a_1$) in its nature. As already implied $7a_1$ to $8a_1$ is too energetic to deserve serious consideration. In summary, among the calculated transitions, 6e and $3b_1 \longrightarrow 4b_1$ are optimal energetically, and both derive intensity from the shared halide σ in-plane character of their donor/acceptor levels. (With these should be included $4e \longrightarrow 7e$, given the substantial in-plane σ character of the donor level.) This is consistent with the strength of the observed band, and fulfills our expectation that metal–halide complexes will exhibit strong absorption in this region with an element of X_σ–M_σ character.[26] The moderate Cl/Br bathochromic shift is also in accord with expectations for such transitions (based on differential Xσ optical electronegativities).

$TcOCl_4$. Most importantly, oxidative electrogeneration of $TcOCl_4$ leads to growth of a new band at 17 200 cm^{-1} which is assigned as the first allowed in-plane $Cl(\pi) \longrightarrow Tc(d\pi)$ process

($6e \longrightarrow 2b_2$, $E_{calc} = 15\,600$ cm^{-1}). On this occasion, a third intense in-plane XMCT band is not expected because the 5e donor orbital possesses less than 2% in-plane π-character in the oxo species (*cf.* Table 6). Thus the calculations reveal that the disposition of the three halide-based e-type donor levels is crucially affected by the identity of the axial ligands, and we suggest that this is the reason for the contrasting optical charge transfer spectra of $[TcNCl_4]^-$ [with *two* in-plane $Cl(\pi/\sigma) \longrightarrow Tc(d\pi)$ transitions] *vs.* $TcOCl_4$ (with *one*). The remaining weak feature in the visible region at 11 300 cm^{-1} is presumably a d–d transition as predicted (Table 5), and tends to confirm the theoretical calculation of the $2b_2/7e$ splitting.

Oxidation of $[TcOCl_4]^-$ is also associated with the expected red-shift in the mid-ultraviolet manifold, provisionally attributed in the Tc^V case at least in part to $3b_1 \longrightarrow 7e$. In Fig. 4(a), this appears as a broad feature at 28 100 cm^{-1} with distinct shoulders at 31 000 and 25 000 cm^{-1}, although the depicted manifold is complicated by the presence of $[TcCl_6]^{2-}$ as an impurity in the reverse electrolysis (reduction) of $TcOCl_4$. According to Table 5, this essentially 'X(vertical)-to-dπ-(vertical)' transition $3b_1 \longrightarrow 7e$ shifts to $E_{calc} = 25\,200$ cm^{-1} in the Tc^{VI} compound (maintaining its favourable donor/acceptor orbital characteristics). Energetically, $6e \longrightarrow 7e$ tends to accompany $3b_1 \longrightarrow 7e$ as noted above. Simultaneously, $4e \longrightarrow 2b_2$, the in-plane $Cl(\sigma/\pi) \longrightarrow Tc(d_{xy})$ transition akin to that described for $[TcNCl_4]^-$ emerges in the same region, with $E_{calc} = 29\,200$ cm^{-1} which means it is estimated to lie above $3b_1 \longrightarrow 7e$. It seems that an adjustment of 2000 to 3000 cm^{-1} to the calculated energies is all that is required if these three excitations are responsible for the absorptions discerned near 28 000 and 31 000 cm^{-1}. Other excitations which might have been implicated are $1a_2 \longrightarrow 7e$ and $5e \longrightarrow 2b_2$ (both very poorly CT-compatible in their make-up), and $7a_1 \longrightarrow 7e$ which is probably too energetic.

Spin–orbit coupled calculations. At a referee's suggestion, we have investigated the inclusion of spin–orbit coupling on pertinent transitions of the $TcYX_4$ chromophore. The most relevant results concern the potential resolution of the three characteristic $e \longrightarrow 2b_2$ excitations into doublets.

In C_{4v} d^1 Tc^{VI}, one-electron promotion from any e-level to singly-occupied d_{xy} (b_2) corresponds to the $^2B_2 \longrightarrow {}^2E$ transition, allowed in x,y polarisation. In double-group notation, $^2B_2 \longrightarrow {}^2E$ becomes $\Gamma_{7\pm} \longrightarrow \Gamma_{7\pm}$, $\Gamma_{6\pm}$. Both excitations are allowed, and correspond naturally enough to the transitions between component orbitals described below.

With spin–orbit coupling included, the singly-occupied $2b_2$ orbital becomes $11e_{3/2}$ while the degenerate e-orbitals divide into an $e_{1/2}$ and $e_{3/2}$ pair. The outcome is summarised in Table 7. One distinct effect is that the calculated transition energies move even lower, because of the relative stabilisation of $11e_{3/2}$. Thus, the centre of each $\Gamma_{7\pm} \longrightarrow \Gamma_{7\pm}$, $\Gamma_{6\pm}$ doublet shifts 1200 cm^{-1}, on average, for $[TcNCl_4]^-$ and $[TcNBr_4]^-$, and 1000 cm^{-1} for $TcOCl_4$. Ligand-derived spin–orbit splitting is more marked for the bromide, as expected. For example, the calculated separation of the leading doublet ($6e \longrightarrow 2b_2$) varies from 300 cm^{-1} in $[TcNCl_4]^-$ (and 500 cm^{-1} in $TcOCl_4$) to 1500 cm^{-1} in $[TcNBr_4]^-$. These seem to be encouraging preliminary results for an entirely first-principles calculation, where no predetermined atomic spin–orbit splitting parameters are employed.[35] However, according to Table 7, the size and even the sign of the splitting appears very dependent on the particular donor orbital, so that the splitting of $5e \longrightarrow 2b_2$ is only 300 cm^{-1} for the same bromo complex. It is not immediately obvious why these splittings are so variable, given that the donor level is almost equally rich in total halide character (≥95%) in all cases. For $TcOCl_4$, where the 5e level is largely quarantined to be ≈90% out-of-plane in character, the calculated splitting of $5e \longrightarrow 2b_2$ dwindles to zero.

Table 7 Effect of spin–orbit coupling on calculated $e \longrightarrow 2b_2$ transition energies (cm^{-1}) for d^1 $TcYX_4$ systems. The difference between listed values is given in parentheses

Transition	$[TcNCl_4]^-$	$[TcNBr_4]^-$	$TcOCl_4$
$6e \longrightarrow 2b_2$	17 300	13 400	15 600
$10e_{3/2} \longrightarrow 11e_{3/2}$	15 800	11 300	13 900
$13e_{1/2} \longrightarrow 11e_{3/2}$	16 100 (+300)	12 800 (+1 500)	14 400 (+500)
$5e \longrightarrow 2b_2$	20 100	15 770	18 700
$8e_{3/2} \longrightarrow 11e_{3/2}$	19 100	14 400	18 000
$12e_{1/2} \longrightarrow 11e_{3/2}$	18 900 (−200)	14 700 (+300)	18 000 (0)
$4e \longrightarrow 2b_2$	29 500	26 200	29 200
$7e_{3/2} \longrightarrow 11e_{3/2}$	28 000	25 500	28 100
$10e_{1/2} \longrightarrow 11e_{3/2}$	28 300 (+300)	24 700 (−800)	28 400 (+300)

Conclusion

The redox chemistry and UV/VIS spectra of d^1 $[TcNX_4]^-$ and d^2 $[TcOX_4]^-$ (X = Cl or Br) have been studied under strictly anhydrous conditions. *In situ* spectroelectrochemical techniques were employed to generate complementary d^2 $[TcNX_4]^{2-}$ and d^1 $TcOCl_4$. This provides a basis for examining the differential axial ligating properties of O^{2-} and N^{3-} in isovalent situations. Bulk oxidation of $[TcOBr_4]^-$ leads to irreversible decomposition. The axial M–Y interactions have been analysed by density functional computations on the eight possible Tc^V and Tc^{VI} species of $\{MYX_4\}$ where X = Cl or Br; Y = N or O, only one of which, $TcOBr_4$, is experimentally unattainable. The observed trends in electrochemical redox potentials and optical XMCT spectra are matched by the computation. For example, the reversible $Tc^{VI/V}$ couple decreases from +1.84 V for $TcOCl_4$ to +0.21 V for $[TcNCl_4]^-$. The composition of the e-type halide-based donor orbitals is particularly sensitive to the nature of the axial ligation. This accounts for the differing complexity in the XMCT manifolds of d^1 $[TcNX_4]^-$ and $TcOCl_4$ when both are dissolved in non-co-ordinating media; it also explains the simplification of the spectra of the nitrido species dissolved in aqueous acid where pseudo-octahedral *trans*-$[TcNCl_4(H_2O)]^-$ and *trans*-$[TcNBr_4(H_2O)]^-$ are formed.

Experimental

Starting materials and general procedures

CAUTION! The isotope ^{99}Tc is a low-energy β-emitter (E_{max} = 0.29 MeV) with a half life of 2.1×10^5 years. All experimental procedures were carried out in a dedicated fume-hood or using sealed glass systems in laboratories approved for low-level radioactive materials. The special techniques followed have been described elsewhere.[36] Potassium pertechnetate was obtained from Amersham International plc. Literature methods provided $[NBu_4][TcO_4]$, $[NBu_4][TcNCl_4]$, $[NBu_4][TcNBr_4]$, $[NBu_4][TcOCl_4]$ and $[NBu_4][TcOBr_4]$.[3,4]

Physical measurements

Cyclic voltammetric- and phase-sensitive alternating current (a.c.) measurements were made with a PAR 170 electrochemistry system. Electrochemical methods, solvents and electrolytes using a specialised electrochemical cell with Pt-electrodes have been described previously.[2,13] Immediately after each experiment ^{99}Tc-compounds were completely decontaminated from the electrochemical cell. After draining all of the radioactive solution from the cell through the Rotaflo-stopcock the cell was rinsed repeatedly with small quantities of acetone until no further activity could be detected in the washings. Following the dismantling of the side-arms from the cell, its interior was soaked with Decon 90 (Decon Laboratories Ltd., England) for 24 h and rinsed thoroughly with distilled water. Finally, the Pt-electrodes were cleaned and reconditioned by treating them with half-concentrated HNO_3.

The electronic absorption spectra (45 000–10 000 cm^{-1}) of solutions were recorded with a Perkin-Elmer λ-9 spectrometer. The spectroelectrochemical techniques using a cryostatted optically transparent thin layer electrode (OTTLE) cell have been described elsewhere.[5] Dichloromethane (Aldrich, analytical grade), used for physical measurements, was refluxed over P_2O_5 for 1 h, before being distilled to a round-bottomed flask containing activated 3 Å molecular sieves. The solvent was degassed by the freeze–thaw method on a vacuum line and subsequently protected from light. Reflectance spectra (5000–35 000 cm^{-1}) were recorded with a Cary 5 spectrometer fitted with a Harrick Praying Mantis sampling attachment. Powdered samples of $[NBu_4][TcX_4]$ were examined both neat and diluted 1:1 with KX, and a Kubelka–Munk correctional function was applied to the measured intensities.

Computational details

Calculations employed the Amsterdam Density Functional (ADF) package developed by Baerends and co-workers[37] and employed the numerical integration scheme of te Velde and Baerends.[38] A triple-ζ STO basis sets was employed for Tc and double-ζ STO basis sets extended with a polarisation function were used for Cl and Br.[39] An auxiliary set of s, p, d, f and g STO basis functions centred on all nuclei was used in order to fit the molecular density and describe accurately the coulomb and exchange potentials in each SCF cycle.[40] Core electrons (up to and including 3d for Tc and Br and 2p for Cl) were treated using the frozen core approximation. The local density approximation[41] (LDA) was employed using the parameterisation of Vosko, Wilk and Nusair.[42] Geometry optimisation was performed using the method developed by Versluis and Ziegler[43] and incorporated the quasi-relativistic correction of Baerends and co-workers.[44] Frequency analyses for the optimised structures yielded all positive values, indicating that the computed geometries correspond to true energy minima. The energies of all LDA-optimised species were recalculated to include the non-local gradient corrections of Becke[45] and Perdew.[46] Spin-polarised, unrestricted calculations were performed on all open-shell species. Transition energies were calculated by the ΔSCF method and are reported incorporating the (post-SCF) gradient corrections of Becke[45] and Perdew.[46] Selected transition energies were recalculated and employing double points groups (see text).

Acknowledgements

We thank Mr. C. J. Tomkins for considerable developmental work on the electrode assembly, Mr. D. Bogsányi for diffuse reflectance measurements, and Dr. Z. Ivanov for access to unpublished spectra in mixed solvents. K. H. M. and G. A. H. acknowledge a federally sponsored R&D Syndicate associated with Tetley Research Ltd. for financial support. S. A. M. was supported by an ANU (R.S.C.) postdoctoral fellowship. S. C. N. thanks the ANU Graduate School, for a Ph.D. scholarship.

References

1 J. Baldas, *Top. Curr. Chem.*, 1996, **176**, 37; *Adv. Inorg. Chem.*, 1994, **41**, 1.
2 K. H. Moock, S. A. Macgregor, G. A. Heath, S. Derrick and R. T. Boeré, *J. Chem. Soc.*, *Dalton Trans.*, 1996, 2067.
3 J. Baldas, J. F. Boas, J. Bonnyman and G. A. Williams, *J. Chem. Soc.*, *Dalton Trans.*, 1984, 2395.
4 W. Preetz and G. Peters, *Z. Naturforsch.*, *Teil B*, 1980, **35**, 1355.
5 C. M. Duff and G. A. Heath, *Inorg. Chem.*, 1991, **30**, 2528.
6 C. M. Duff and G. A. Heath, *J. Chem. Soc.*, *Dalton Trans.*, 1991, 2401.
7 J. B. Raynor, T. J. Kemp and A. M. Thyer, *Inorg. Chim. Acta*, 1992, **193**, 191; R. Kirmse, K. Kohler, U. Abram, R. Bottcher, L. Golic and E. de Boer, *Chem. Phys.*, 1990, **143**, 75; K. Kohler, R. Kirmse, R. Bottcher, U. Abram, M. C. M. Gribnau, C. P. Keijzers and E. de Boer, *Chem. Phys.*, 1990, **143**, 83.
8 A. Neuhaus, A. Veldkamp and G. Frenking, *Inorg. Chem.*, 1994, **33**, 5278.
9 P. A. Reynolds, B. N. Figgis, J. B. Forsyth and F. Tasset, *J. Chem. Soc.*, *Dalton Trans.*, 1997, 1447.
10 K. H. Moock and S. A. Macgregor, 1997, *Inorg. Chem.*, 1998, in the press.
11 S. Brownstein, G. A. Heath, A. Sengupta and D. W. A. Sharp, *J. Chem. Soc.*, *Chem. Commun.*, 1983, 669.
12 G. A. Heath, K. H. Moock, D. W. A. Sharp and L. J. Yellowlees, *J. Chem. Soc.*, *Chem. Commun.*, 1985, 1503.
13 K. H. Moock and M. H. Rock, *J. Chem. Soc.*, *Dalton Trans.*, 1993, 2459.
14 R. W. Thomas, M. J. Heeg, R. C. Elder and E. Deutsch, *Inorg. Chem.*, 1985, **24**, 1472.
15 J. Baldas, J. F. Boas and J. Bonnyman, *J. Chem. Soc.*, *Dalton Trans.*, 1987, 1721; J. Baldas, J. F. Boas, B. D. James and Z. Ivanov, *Transition Met. Chem.*, 1997, **22**, 74.
16 J. Baldas, J. Bonnyman and G. A. Williams, *Aust. J. Chem.*, 1985, **38**, 215.
17 R. Colton and I. B. Tomkins, *Aust. J. Chem.*, 1968, **21**, 1981; A. Guest and C. J. L. Lock, *Can. J. Chem.*, 1972, **50**, 1807.
18 J. Baldas and S. F. Colmanet, *Aust. J. Chem.*, 1989, **42**, 1155.
19 R. Hübener and U. Abram, *Z. Anorg. Allg. Chem.*, 1992, **617**, 96.
20 P. D. Lyne and D. M. P. Mingos, *J. Chem. Soc.*, *Dalton Trans.*, 1995, 1635.
21 R. J. Deeth, *J. Chem. Soc.*, *Dalton Trans.*, 1991, 1895.
22 B. N. Figgis, P. A. Reynolds and J. W. Cable, *J. Chem. Phys.*, 1993, **98**, 7743.
23 M. D. Carducci, C. Brown, E. I. Soloman and J. H. Enemark, *J. Am. Chem. Soc.*, 1994, **116**, 11 856; D. M. Sabel and A. A. Gewirth, *Inorg. Chem.*, 1994, **33**, 148; D. Collison, *J. Chem. Soc.*, *Dalton Trans.*, 1990, 2999.
24 E. I. Solomon, *Comments Inorg. Chem.*, 1984, **3**, 227.
25 A. Van der Avoird and P. Ros, *Theor. Chim. Acta*, 1966, 13.
26 G. A. Heath and J. E. McGrady, *J. Chem. Soc.*, *Dalton Trans.*, 1994, 3759.
27 K. H. Moock, Ph.D. Thesis, University of Glasgow, 1985, p. 176.
28 S. C. Nissen, Ph.D. Thesis, Australian National University, 1997; L. J. Yellowlees and K. H. Moock, unpublished measurements.
29 A. B. P. Lever, *Inorg. Chem.*, 1990, **29**, 1271.
30 J. Baldas, J. F. Boas, Z. Ivanov and B. D. James, *Inorg. Chim. Acta*, 1993, **204**, 199.
31 G. A. Heath and D. G. Humphrey, *J. Chem. Soc.*, *Chem. Commun.*, 1991, 1668.
32 A. B. P. Lever, *Inorganic Electronic Spectroscopy*, Elsevier, New York, 1984, 2nd edn., p. 739.
33 G. A. Heath and R. G. Raptis, *Inorg. Chem.*, 1991, **30**, 4108; J. E. McGrady, Ph.D. Thesis, Australian National University, 1994.
34 J. Baldas, B. D. James and Z. Ivanov, in preparation.
35 J. G. Snijders, E. J. Baerends and P. Ros, *Mol. Phys.*, 1979, **38**, 1909.
36 J. C. Bryan, A. K. Burrell, M. M. Miller, W. H. Smith, C. J. Burns and A. P. Sattelberger, *Polyhedron*, 1993, **22**, 1695.
37 E. J. Baerends, D. E. Ellis and P. Ros, *Chem. Phys.*, 1973, **2**, 41; E. J. Baerends, J. G. Snijders, C. A. de Lange and G. Jonkers, *Local Density Approximations in Quantum Chemistry and Solid State Physics*, eds. J. P. Dahl and J. Avery, Plenum, New York, 1984.
38 G. te Velde and E. J. Baerends, *J. Comp. Phys.*, 1992, **99**, 84.
39 J. G. Snijders, E. J. Baerends and P. Vernooijs, *At. Data Nucl. Data Tables*, 1982, **26**, 483; P. Vernooijs, J. G. Snijders and E. J. Baerends, *Slater Type Basis Functions for the whole Periodic System*, Internal Report, Free University of Amsterdam, 1981.
40 J. Krijn and E. J. Baerends, *Fit Functions in the HFS-method*, Internal Report, Free University of Amsterdam, 1984.
41 O. Gunnarsson, B. I. Lundqvist and J. W. Wilkins, *Phys. Rev. B*, 1974, **10**, 1319; O. Gunnarsson and B. I. Lundqvist, *Phys. Rev. B*, 1976, **13**, 4274; O. Gunnarsson, M. Jonson and B. I. Lundqvist, *Phys. Rev. B*, 1979, **20**, 3136.
42 S. H. Vosko, L. Wilk and M. Nusair, *Can. J. Phys.*, 1980, **58**, 1200.
43 L. Versluis and T. Ziegler, *J. Chem. Phys.*, 1988, **88**, 322.
44 T. Ziegler, V. Tschinke, E. J. Baerends, J. G. Snijders and W. Ravenek, *J. Phys. Chem.*, 1989, **93**, 3050; R. van Leeuwen, E. van Lenthe, J. G. Snijders and E. J. Baerends, *J. Chem. Phys.*, 1994, **101**, 1272.
45 A. D. Becke, *J. Chem. Phys.*, 1986, **84**, 4524.
46 J. P. Perdew, *Phys. Rev. B*, 1986, **33**, 8822.

Received 3rd *April* 1998; *Paper* 8/02559B